On Epitaxial Electrodeposition of Co, Cu and Ru for Interconnect Applications

Katayun Barmak[1], Ryan R. Gusley[2]

[1]Department of Applied Physics and Applied Mathematics, Columbia University, New York, New York 10027, United States of America

[2]Department of Chemical Engineering, Columbia University, New York, New York 10027, United States of America

Abstract

Epitaxial electrodeposition of Co, Cu and Ru is compared and contrasted. The seed layer for electrodeposition of all three metals was an epitaxial Ru(0001) film that was deposited at an elevated temperature onto a sapphire(0001) substrate and annealed post deposition. The epitaxial orientation relationship of the electrodeposited film and the seed layer, the epitaxial misfit strain, the role of symmetry of the seed layer versus the electrodepositing layer is addressed. In addition, the impact of underpotential deposition on film nucleation, and the growth morphology of the films is discussed. It is shown that epitaxial electrodeposition of metallic films to thicknesses of tens of nanometers is readily achievable.

Introduction

As the critical dimensions of copper (Cu) interconnects become comparable to or less than the electron mean free path of the metal (39.9 nm at room temperature), a rise in resistivity is observed.[1-5] This phenomenon, first observed by Thomson in 1901 and termed the resistivity size-effect, is the result of electron scattering at grain boundaries and surfaces.[6] Given that electron scattering from grain boundaries is a major contributor to the resistivity rise, this work summarizes recent efforts on room-temperature epitaxial electrodeposition of single crystal and

bicrystal films tens of nanometers in thickness, using Co, Cu and Ru as three metals of choice.[7-10]

Epitaxial metals are routinely obtained by vacuum deposition, but require temperatures of several hundred degrees. In contrast, epitaxial electrodeposition of metals can be done at room temperature, but it requires a conductive seed layer. Electrodeposition techniques such as surfactant-mediated growth (SMG), defect-mediated growth (DMG), and growth via surface-limited redox replacement (SLRR) have previously demonstrated 2-D growth of metals films. [11-15] These techniques, however, often involve the inclusion of a surfactant in the deposition solution, most commonly toxic lead (Pb), and/or require a manipulation of applied potential throughout the deposition process. The work presented here demonstrates direct current (DC) electroplating as capable of growing epitaxial metal films without the use of surfactants. The conductive seed layer for the work presented here was Ru(0001) obtained by sputter deposition onto sapphire(0001) single crystal substrates. The epitaxial orientation relationship between the seed layer and the electrodeposited layers, the role of symmetry of the seed layer, the epitaxial misfit strain, the impact of underpotential deposition on film nucleation, and the growth morphology of the depositing layer is discussed.

Methodology

Film Preparation. – The seed layers were prepared by sputter deposition. Both polycrystalline and single crystal, epitaxial Ru seed layers were used in order to allow for comparisons of the microstructure of the resultant electrodeposited layers. For the polycrystalline Ru seed layer, the substrate was an oxidized Si(001) wafer coated with a 4 nm-thick reactively-sputtered TaN layer. For the epitaxial Ru(0001) seed layer, the substrate was sapphire(0001), and the films were

annealed following deposition. For the electrodeposition of Co, Cu and Ru on the seed layers, the electrolytes and the deposition parameters are briefly described in the figure captions where relevant. Additional details of the seed and electrodeposited layer preparation are given in [7-10, 16-20].

Characterization of electrodeposited films. – The films were characterized using X-ray reflectivity (XRR), X-ray diffraction (XRD), scanning electron microscopy (SEM), electron back scatter diffraction (EBSD), scanning/transmission electron microscopy (S/TEM), selected area electron diffraction (SADP), and energy dispersive X-ray spectroscopy (EDS). Cross-sectional samples for S/TEM were prepared by focused ion beam milling. Additional details are given in [7-10, 16-20].

Results

Orientation relationship and misfit strain. – An important consideration in epitaxial deposition is the orientation relationship (OR) between the substrate and the deposited layers, whether vacuum deposited or electrodeposited, based on which the epitaxial misfit strain can then be calculated. X-ray ϕ-scans are a very convenient and non-destructive method for determining the OR. Figure 1 presents the diffracted intensities for a Cu film electrodeposited on a Ru(0001) seed layer that was sputter deposited on a sapphire(0001) substrate. The 30-degree displacement between the Ru $\{11\bar{2}2\}$ and Al_2O_3 $\{11\bar{2}6\}$ peaks indicates that the OR between Ru and sapphire is the 30-degree rotated honeycomb, i.e., rotated hexagon, in agreement with prior reports.[16-20] This rotation allows the epitaxial misfit strain between Ru and sapphire to be reduced to 1.5% from 75.9% for a hexagon-on-hexagon OR.[20] By contrast, given that Cu is face-centered cubic, the 30-degree

displacement of the Cu $\{111\}$ and Ru $\{11\bar{2}2\}$ peaks in Fig. 1 indicates that the OR between Cu and Ru is hexagon-on-hexagon.

Using X-ray ϕ-scans, the OR for Co(0001) on Ru(0001) seed is also found to be hexagon-on-hexagon, and is shown schematically in Fig. 2. For this OR, Co$[0001]$|| Ru$[0001]$and Co $[2\bar{1}\bar{1}0]$|| Ru$[2\bar{1}\bar{1}0]$, allowing us to calculate the misfit strain as:

$$\varepsilon_{Co/Ru} = \frac{d^{Ru}_{10\bar{1}0} - d^{Co}_{10\bar{1}0}}{d^{Co}_{10\bar{1}0}} = 7.9\% \quad , \qquad (1)$$

where the d's are the interplanar spacings (see Fig. 1). These spacings are calculated using the 293.15 K lattice parameters of Ru and Co, which are $a_{Ru} = 2.7059$ Å, $c_{Ru} = 4.2819$ Å and $a_{Co} = 2.5071$ Å, $c_{Co} = 4.0695$ Å, respectively, and it has been assumed that the Ru layer has fully relaxed its misfit strain relative to sapphire following the post-sputter deposition annealing treatment and has adopted its

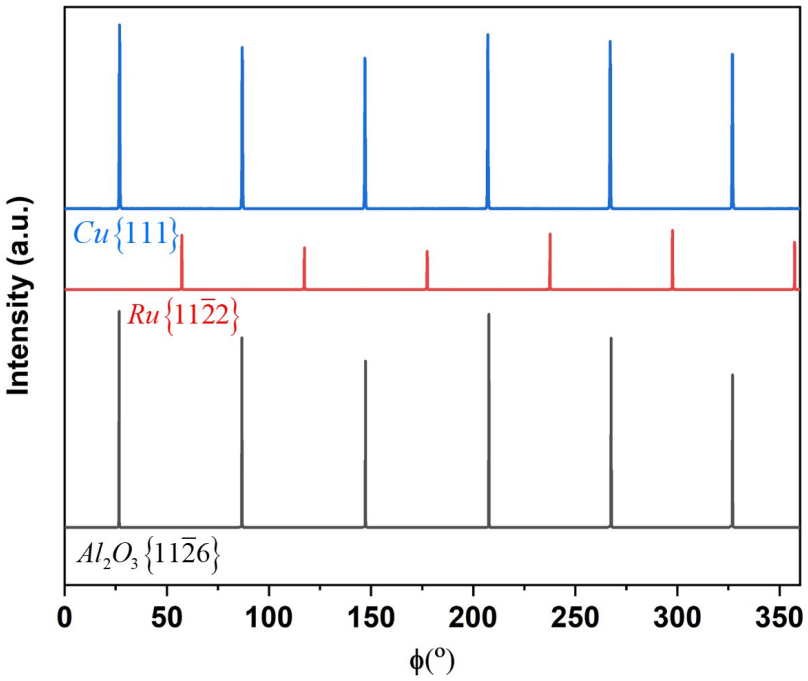

Fig. 1 – Diffracted X-ray intensity for given family of crystallographic planes is plotted versus the sample rotation angle about the substrate normal, ϕ, for Cu electrodeposited at -350 μAcm^{-2} for 1200 s from a solution of 2 mM $CuSO_4$, 0.5 M H_2SO_4 and 1.41 mM KCl on a 30-nm thick Ru(0001) seed layer that was sputter deposited on sapphire(0001). The plots have been displaced for clarity.

bulk lattice parameters.[7,8, 21] In the case of an unrelaxed Ru seed layer, the misfit strain would be 9.6%.

For the hexagon-on-hexagon OR of Cu(111) on Ru(0001) [10], $\mathrm{Cu}[111] \| \mathrm{Ru}[0001]$ and $\mathrm{Cu}[1\bar{1}0] \| \mathrm{Ru}[11\bar{2}0]$ leading to a tensile misfit strain for the case of a fully relaxed Ru layer relative to the sapphire substrate of:

$$\varepsilon_{\mathrm{Cu/Ru}} = \frac{d^{\mathrm{Ru}}_{11\bar{2}0} - d^{\mathrm{Cu}}_{2\bar{2}0}}{d^{\mathrm{Cu}}_{2\bar{2}0}} = 5.9\%. \qquad (2)$$

where the *d*'s are again the interplanar spacings and are calculated using the 293.15 K lattice parameters, which for Cu is $a_{\mathrm{Cu}} = 3.6150$ Å .[16] In the case of an unrelaxed Ru seed layer, the misfit strain would be 7.4%.

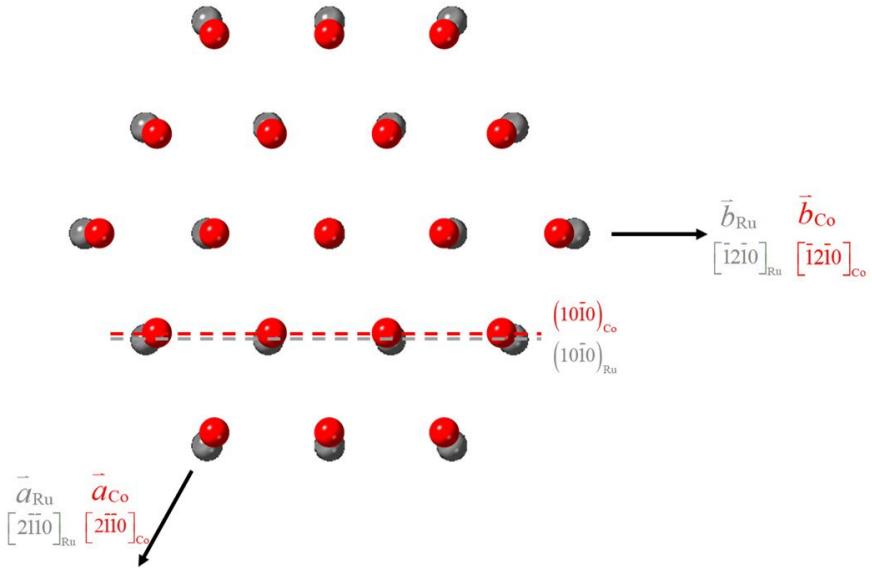

Fig. 2 – Schematic representation of the epitaxial orientation relationship between Co(0001) and Ru(0001). The [0001] direction for both Co and Ru points out of the page. The until cell of Ru is defined in by placing a Ru atom at the origin (0,0,0) in the basal plane. Only the single layers of the elements at the interface are shown for clarity.

With respect to the number of variants for a given OR, the electrodeposited Co layer and the Ru seed layer are both hexagonal close packed metals with six fold symmetry along the c-axis, i.e., the [0001] direction,

and therefore there is only one variant. By contrast for Cu, the symmetry along the [111] direction is three-fold, and consquently the electrodeposited layer comprises two crystallographic variants that are 60°-misoriented relative each other. In other words, the electrodepsoited Cu layer is bicrystalline whereas the electrodeposited Co layer is single crystalline.[10]

For Ru electrodeposited on Ru, there is clearly no misfit strain and the OR is hexagon-on-hexagon. However, it was shown that electrodeposition of Ru on a Ru(0001) seed layer, though epitaxial, does not yield a fully dense layer.[9]

Nucleation, growth.- For epitaxial electrodeposition of films, two regimes of deposition should be noted. These are overpotential deposition (OPD) and underpotential deposition (UPD), as shown schematically in Fig. 3. OPD is the regime where the potential is negative of the Nernst

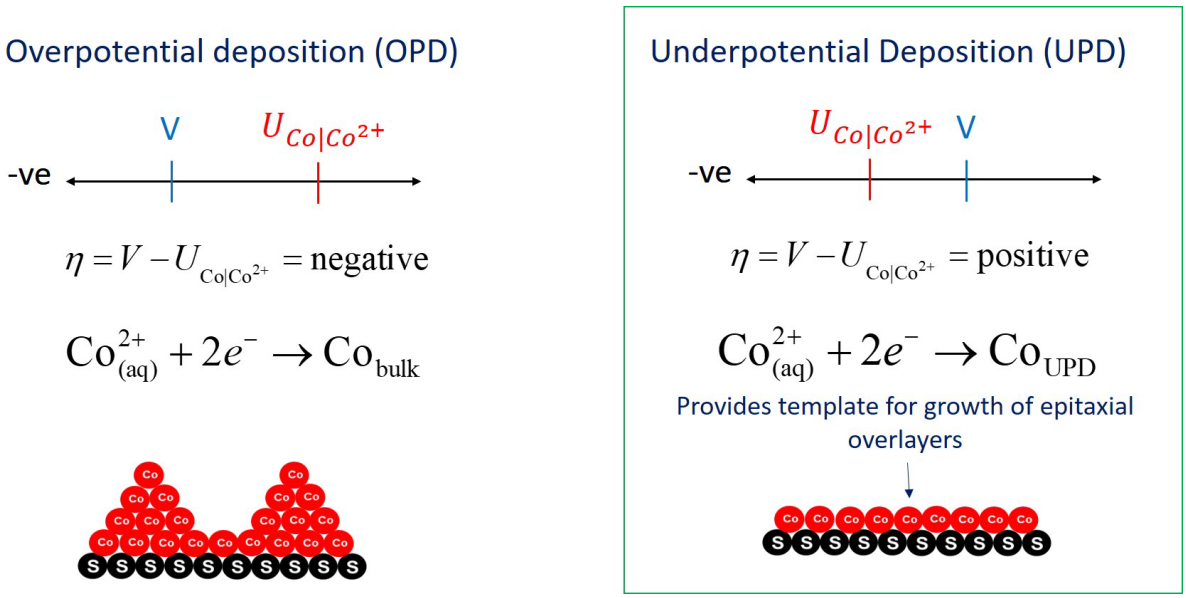

Fig. 3 – Schematic representing overpotential deposition (left), i.e., deposition at potentials, V, negative of the Nernst potential, U, and underpotential deposition (right), i.e., deposition at potentials positive of the Nernst potential, using the deposition of Co on a conductive seed layer (S) as an example.

potential for the given electrolyte; it proceeds by nucleation and growth of individual domains that

then coalesce to form a contiguous layer (Fig. 3). The current transient for this regime exhibits a peak, as seen in Fig. 4. Here, the Ru seed layer was held for 20 seconds at -0.4 V (η = +180 mV, where η is the overpotential) before stepping the potential to -0.8 V(η = -250 mV) for Co OPD.

The second deposition regime of importance to epitaxial electrodeposition, the UPD regime, is a self-limiting regime that results in the deposition of a sub/monolayer of the depositing metal at a potential positive of the Nernst potential (Fig. 3).[22,23] This layer then provides a template for epitaxial electrodeposition of overlayers in the OPD regime

The current transient in the UPD regime shows a continuous decay with increasing time, as seen in Fig. 4. Here, the Ru seed layer was held for 20 seconds at -0.56 V (η = +20 mV) before stepping the potential to -0.8 V(η = -250 mV) for Co OPD. The inset in Fig. 4 presents the change in the current transient with increasing hold time from 0.1 to 10 seconds at η = +20 mV, before the step to the OPD potential. The

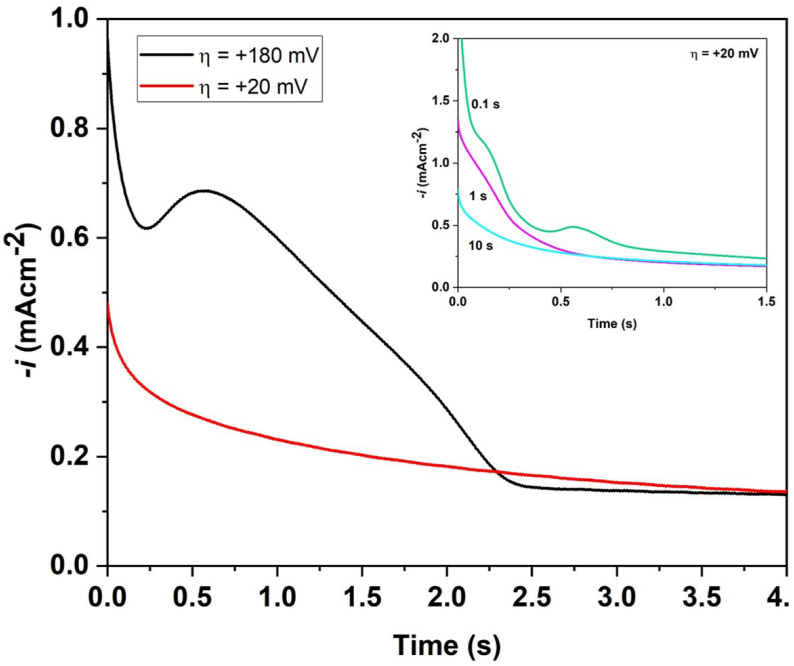

Fig. 4 – Current transients for Co electrodeposition on a 60-nm thick Ru(0001) seed layer at -0.8 V (η = -250 mV) after initial holds of, respectively, -0.4 V (η = +180 mV) and -0.56 V (η = +20 mV) for 20 seconds.[7] The deposition solution is 1 mM $CoSO_4$, 0.125 mM H_2SO_4, 10 mM K_2SO4, and 0.1 mM KCl and the solution pH was 3.8. The inset shows the current transients for different hold times for η = +20 mV prior to the step to -0.8 V. The deposition solution used a higher concentration of 0.25 mM H_2SO_4 resulting in a solution pH of 3.6. Figure is reproduced with modification from [7].

change in the current transient with increasing hold time evidences the growth of the template layer, which reaches its maximum coverage at 10s.

The potential-step experiments, as in Fig. 4, are just one method by which to demonstrate the role of UPD in the formation of the template layer for epitaxial electrodeposition. In [7], cyclic voltammetry was used to show UPD of both Co and Cu on the Ru seed layer. The UPD template layer also forms under conditions where the deposition is done at a fixed current density.

Morphology of the electrodeposit. – To examine the morphology of the epitaxial electrodeposits, Co, Cu and Ru were deposited under constant current conditions. To begin, it is useful to consider the morphology of Co electrodeposited on polycrystalline Ru, presented in Fig. 5. The top surface of the Ru layer is clearly

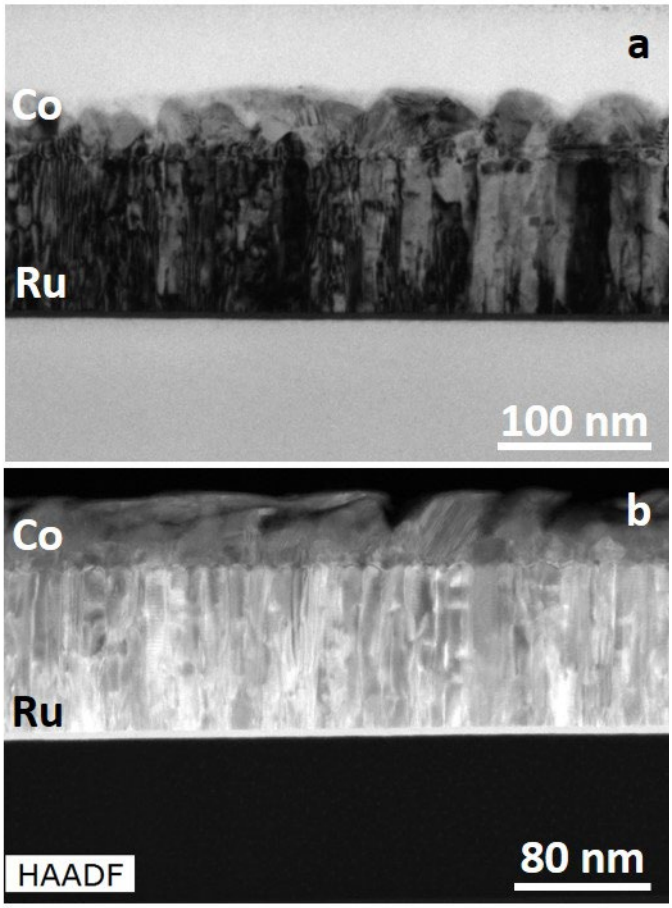

Fig. 5 – (a) Bright-field transmission electron micrograph and (b) high-angle annular dark-field scanning transmission electron micrograph of Co electrodeposited galvanostatically from a solution of 1 mM $CoSO_4$, 0.125 mM H_2SO_4, 10 mM K_2SO4, and 0.1 mM KCl at -100 μAcm^{-2} on a nominally 100 nm-thick polycrystalline seed layer that was sputter deposited onto a reactively sputter deposited TaN layer on oxidized Si(001). The TaN is clearly seen as a thin layer of uniform light contrast above the oxide layer and below the Ru layer in (b). The oxide layer appears as a black layer in (b), and as a light grey layer in (b). The polycrystalline Ru layer is [001] fiber-textured.

faceted, more easily seen in the high-angle annular dark-field (HAADF), image of Fig. 5b. The facetted surface of the polycrystalline Ru layer leads to the growth of a rough, polycrystalline Co layer, more clearly seen in the bright-field transmission electron micrograph of Fig. 5a. By contrast, Fig. 6a, high angle annular dark field image, and Fig. 6b, a montage of the elemental maps of Co and Ru corresponding to Fig. 6a, show that electrodeposition of Co on the epitaxial Ru(0001) seed yields a planar Co(0001) layer several tens of nanometer in thickness, before the Co roughens and facets to a similar extent as Co grown on polycrystalline Ru. The roughening of the Co layer provides a means to relieve the misfit strain energy, and the thickness at which significant roughening occurs depends on the magnitude of the misfit strain, decreasing with increasing misfit strain.[8] Layer-by-layer growth that transitions to 3-D growth beyond a certain critical thickness is identified as Stranski-Krastanov growth.[24]

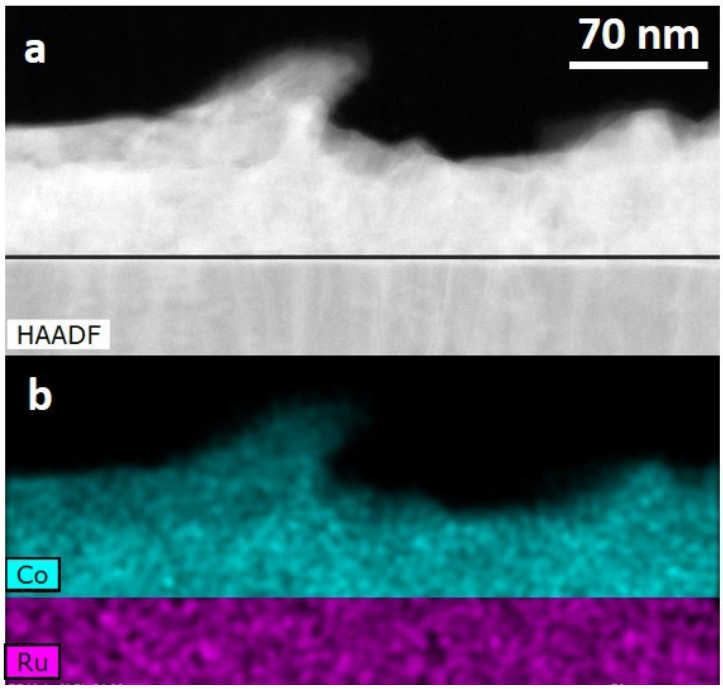

Fig. 6 – (a) High-angle annular dark-field scanning transmission electron micrograph and (b) montage of energy dispersive X-ray spectroscopy elemental maps of Co epitaxially electrodeposited at -100 μAcm^{-2} from a solution of 1 mM $CoSO_4$, 0.125 mM H_2SO_4, 10 mM K_2SO4, and 0.1 mM KCl on a 60-nm thick Ru(0001) seed layer. The black line in (a) is a guide to the eye marking the Co/Ru interface.

Though Cu and Co both have a tensile misfit strain relative to Ru, the epitaxial electrodeposition of Cu on Ru(0001) seed at constant current density begins as crystallographically

facetted islands, as shown in the plan view scanning electron micrograph and the corresponding elemental maps in Figs. 7a-c, and the bright-field transmission electron images of a cross-sectional image in Fig. 8a. With increasing deposition time, the Cu layer becomes planar and contiguous as seen in Fig. 8b. A planar deposition is maintained up to a Cu thickness of 200 nm. However, beyond this thickness a re-emergence of the faceted islands of Cu occurs.[10]

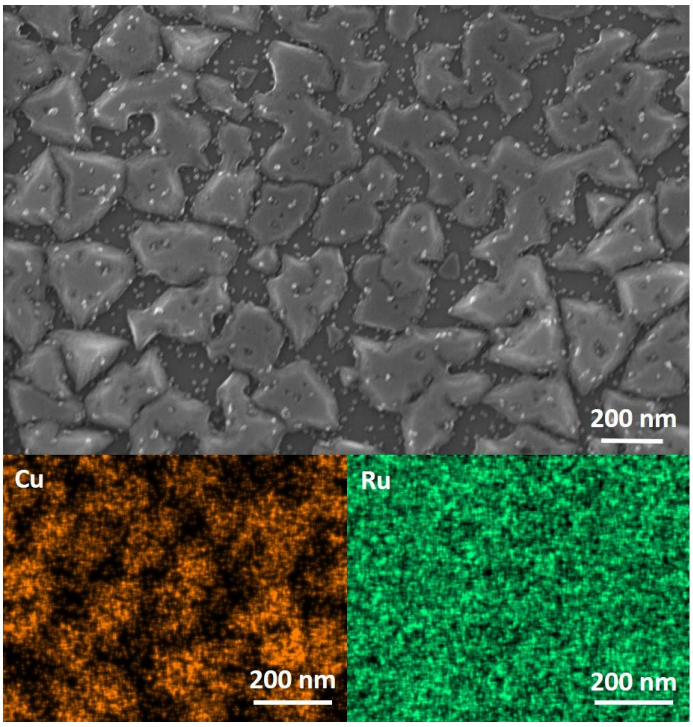

Fig. 7 – Scanning electron microscopy image and energy dispersive X-ray spectroscopy elemental maps for Cu epitaxially electrodeposited at -350 μAcm^{-2} from a 2 mM $CuSO_4$, 0.5 M H_2SO_4, and 1.41 mM KCl solution onto a 30-nm thick Ru(0001) seed layer.

Ru also electrodeposits epitaxially on Ru(0001) using a plating solution of 2 g L^{-1} ruthenium(III) nitrosyl sulfate ($[Ru(NO)]_2(SO_4)_3$) and 20 g L^{-1} sulfuric acid. However, as was shown in extensive detail in [9], the deposited layer is porous. The density of the porous deposit increases with increasing current density up to a maximum density that then remains constant with increasing current density but never reaches the bulk density of Ru of 12.414 gcm^{-3}.

Discussion

The preceding sections have shown that epitaxial electrodeposition can be readily achieved at room temperature to generate on a Ru(0001) seed layers single crystal films of Co and bicrystal films of Cu that are tens of nanometers in thickness. This despite the very large tensile misfit strains

of several percent (5-10%) for Co(0001) and Cu(111) relative to the Ru(0001) seed that was used for these studies.[7,8,10]

It was also shown that UPD plays a critical rule in the formation of the template layer on the epitaxial, conductive seed layer.[7,8,10] The template layer then allows the epitaxial growth of the electrodeposit during OPD or during deposition at constant current density.

For the case of bicrystalline Cu(111) films electrodeposited on Ru(0001), ref. [10] showed that these films had lower resistivities than for Cu films of the same thickness deposited on polycrystalline Ru films. The films were annealed at 400 °C for 1 h in flowing Ar/3%H_2 prior to resistivity measurements.

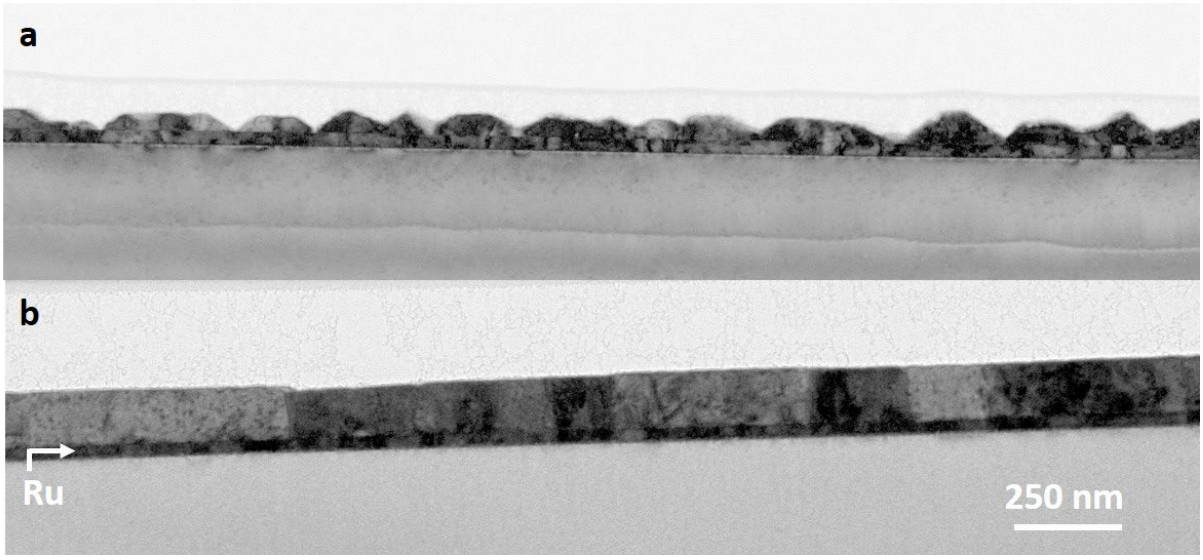

Fig. 8 – Transmission electron micrographs of cross sections of nominally (a) 50 and (b) 200 nm-thick Cu films epitaxially electrodeposited at -350 μAcm^{-2} from a solution of 2 mM $CuSO_4$, 0.5 M H_2SO_4, and 1.41 mM KCl onto a 30-nm thick Ru(0001) seed layer. The Ru seed layer is marked with a white arrow in (b), but is also present in (a).

Conclusions

The work presented here demonstrates that with the use of an epitaxial, single crystal seed layer, epitaxial electrodeposition of metallic layers is easily achieved, so long as a template layer of the electrodeposited layer is formed in the regime of underpotential deposition. This template layer then promotes the epitaxial growth of the electrodepositing overlayer. Although the epitaxial seed layer was limited to Ru(0001), and only electrodeposition of Co, Cu and Ru were presented, the approach is applicable to many other seed layer/electrodeposited layer combinations. However, successful implementation of epitaxial electrodeposition for interconnect applications will require a great deal more future work in optimizing not only the plating solution and deposition parameters, but also the crystal structure, crystallographic orientation, lattice parameter and work function of the seed layer.

Acknowledgments

Funding support by Semiconductor Research Corporation (tasks 2764.001 and 2764.003), the National Science Foundation (ECCS-1740270 and 1740228), and the Air Force Office of Scientific Research (AFOSR FA9550-18-1-0063 and FA9550-19-1-0156) is gratefully acknowledged. The microscopy for this work was carried out in part in part by K. Sentosun and A. Zangiabadi in the Electron Microscopy and Shared Materials Characterization Laboratories of Columbia Nano Initiative (CNI) Facilities at Columbia University.

ORCID

Katayun Barmak https://orcid.org/0000-0003-0070-158X

Ryan R. Gusley https://orcid.org/0000-0001-7015-2921

References

1. W. Steinhögl, G. Schinlder, G. Steinlesberger, M. Traving, and M. Engelhardt, *J. Appl. Phys.* **97**, 023706 (2005).
2. D. Josell, S. H. Brongersma, Z. Tőkei, *Annu. Rev. Mater. Res.* **39**, 231 (2009).
3. T. Sun, Bo Yao, A. P. Warren, K. Barmak, M. F. Toney, R. E. Peale, and K. R. Coffey, *Phys. Rev. B* **81**, 155454 (2010).
4. K. Barmak, A. Darbal, K. J. Ganesh and P. J. Ferreira, T. Sun, B. Yao, A. P. Warren, K. R. Coffey, J. M. Rickman, *J. Vac. Sci. Technol.* **A 32**, 061503 (2014).
5. K. Barmak, X. Liu, A. Darbal, D. Choi, N. T. Nuhfer, T. Sun, A. P. Warren, K. R. Coffey, M. F. Toney, *J. Appl. Phys.* **120**, 065106 (2016).
6. J. J. Thomson, *Proc. Camb. Philos. Soc.* **11**, 120 (1901).
7. R. Gusley, K. Sentosun, S. Ezzat, K. R. Coffey, A. C. West, K. Barmak, *J. Electrochem. Soc*. **166,** D875-D881 (2019).
8. R. Gusley, S. Ezzat, K. R. Coffey, A. C. West, K. Barmak, *J. Electrochem. Soc.* **167** 162503 (2020).
9. R. Gusley, Q. Cumston, K. R. Coffey, A. C. West, K. Barmak, *J. Electrochem. Soc.* **168**, 052504 (2021).
10. R. Gusley, Q. Cumston, K. R. Coffey, A. C. West, K. Barmak, *J. Appl. Phys.* **130**, 135301 (2021) and **131**, 209903 (2022).
11. Seongpil Hwang, A. Ilwhan Oh, and J. Kwak, *J. Am. Chem Soc.* **123** (2001).
12. K. Sieradzki, S. Brankovic, Dimitrov, and N. Dimitrov, *Science*, **284**, 138 (1999).
13. D. Wu, D. J. Solanki, A. Joi, Y. Dordi, N. Dole, D. Litvnov, and S. R. Brankovic, *J. Electrochem. Soc.*, **166**, D3013 (2019)

14. K. Venkatraman, Y. Dordi, and R. Akolkar, *J. Electrochem. Soc.*, **164**, D104 (2017).

15. K. Venkatraman, R. Gusley, L. Yu, Y. Dordi, and R. Akolkar, *J. Electrochem. Soc.*, **164**, D3008 (2016).

16. S.Yamada, Y. Nishibe, M. Saizaki, H. Kitajima, S. Ohtsubo, A. Morimoto, T.Shimizu, K. Ishida, and Y. Masaki, Jpn. J. Appl. Phys. **41**, L206 (2002).

17. E. Milosevic, S. Kerdsongpanya, A. Zangiabadi, K. Barmak, K.R. Coffey, and D. Gall, J. Appl. Phys. **124**, 165105 (2018).

18. S. Ezzat, P. Doss Mani, A. Khaniya, W. Kaden, D. Gall, K. Barmak, K. R. Coffey, *J. Vacuum Sci. Technol*. A **37**, 031516 (2019).

19. K. Barmak, S. Ezzat, R. Gusley, A. Jog, S. Kerdsongpanya, A. Khanya, E. Milosevic, W. Richardson, K.Sentosun, A. Zangiabadi, D. Gall, W. E. Kaden, E. R. Mucciolo, P. K. Schelling, A. C. West, K. R. Coffey, *J. Vac. Sci. Technol.* A **38**, 033406 (2020).

20. K. Barmak, K. Sentosun, A. Zangiabadi, E. Milosevic, D. Gall, M. Zecevic, R. Lebensohn, J. Floro, *J. Appl. Phys.* **128**, 045304 (2020).

21. J.W. Arblaster, *Selected Values of the Crystallographic Properties of Elements* (ASM, Materials Park, 2018).

22. D. M. Kolb, M. Przasnyski, and H. Gerischer, *J. Electroanal. Chem. Interfacial Electrochem.*, **54**, 25 (1974).

23. N. Bogolowski, S. Huxter, A.A. Abd-El-Latif, G.A. Attard, H. Baltruschat, *J. Electroanal. Chem. Interfacial Electrochem.*, **646**, 68 (2010).

24. A. Baskaran and P. Smereka, *J. Appl. Phys.*, **111**, 044321 (2012).